Human Molecular Genetics, 2008, Vol. 17, No. 16 **2474–2485**
doi:10.1093/hmg/ddn147
Advance Access published on May 10, 2008

The Primary open-angle glaucoma gene *WDR36* functions in ribosomal RNA processing and interacts with the p53 stress–response pathway

Jonathan M. Skarie and Brian A. Link*

Department of Cell Biology, Neurobiology and Anatomy, Medical College of Wisconsin, Milwaukee, WI, USA

Received February 25, 2008; Revised and Accepted May 7, 2008

Primary open-angle glaucoma (POAG) is a genetically complex neuropathy that affects retinal ganglion cells and is a leading cause of blindness worldwide. *WDR36*, a gene of unknown function, was recently identified as causative for POAG at locus GLC1G. Subsequent studies found disease-associated variants in control populations, leaving the role of *WDR36* in this disease unclear. To address this issue, we determined the function of WDR36. We studied Wdr36 in zebrafish and found it is the functional homolog of yeast Utp21. Utp21 is cell essential and functions in the nucleolar processing of 18S rRNA, which is required for ribosome biogenesis. Evidence for functional homology comes from sequence alignment, ubiquitous expression, subcellular localization to the nucleolus and loss-of-function phenotypes that include defects in 18S rRNA processing and abnormal nucleolar morphology. Additionally, we show that loss of Wdr36 function leads to an activation of the p53 stress–response pathway, suggesting that co-inheritance of defects in p53 pathway genes may influence the impact of *WDR36* variants on POAG. Although these results overall do not provide evidence for or against a role of *WDR36* in POAG, they do provide important baseline information for future studies.

INTRODUCTION

Glaucomas are a heterogeneous group of blinding neuropathies that result in retinal ganglion cell (RGC) death, visual field deficits and optic nerve atrophy (1). They are currently a leading cause of blindness worldwide, and estimates predict 60 million people will be diagnosed with the disease by 2010 (2). The most prevalent form of glaucoma is primary open-angle glaucoma (POAG), the incidence of which increases with advancing age (3). POAG is a complex disease, with multiple genetic and environmental factors interacting to cause disease (1,4,5). High intraocular pressure (IOP) is the greatest risk factor for developing glaucoma, and is thought to result from defects in aqueous humor drainage within the anterior segment of the eye. It is unknown exactly how elevated IOP impacts POAG. Currently, the most accepted hypothesis is that elevated pressure in the anterior chamber of the eye is translated to the posterior chamber, creating stress at the optic nerve head and, ultimately, resulting in death of RGCs (6–11). Though high IOP is the most common risk factor, it is not required for the development of POAG. About one-third of cases occur in normal tension patients (IOP < 22 mmHg) (12). Together, this suggests that glaucoma can result from insults to the drainage structures in the anterior chamber and/or from intrinsic defects in RGCs (1).

Determining the genetic risk factors of POAG has been an area of intense study, but the complex nature of the disease has made the search very difficult (13). Through human genetic screens, at least 20 loci have been found that link to POAG, but causative genes have only been reported for three (13). These genes are *MYOCILIN*, *OPTINEURIN* and *WDR36*. Genetically, both *MYOCILIN* and *OPTINEURIN* have been well established in influencing POAG, but the endogenous functions of these proteins as well as the exact mechanism by which they cause disease are unknown (1). *MYOCILIN* is the causative gene at locus GLC1A, and is associated with high IOP cases of POAG (13,14). MYOCILIN is expressed at high levels in trabecular meshwork cells, and it is thought that disease causing mutations result in cellular

*To whom correspondence should be addressed at: Department of Cell Biology, Neurobiology and Anatomy, Medical College of Wisconsin, 8701 Watertown Plank Road BSB 405, Milwaukee, WI 53226, USA. Tel: +1 4144568072; Fax: +1 4144566517; Email: blink@mcw.edu

dysfunction as a result of blocked secretion and ectopic peroxisome targeting (15–20). Compromised trabecular meshwork cells result in raised IOP, which then contributes to glaucoma. *OPTINEURIN* is the causative gene at locus GLC1E and was found to cause normal-tension POAG (21). Genetic studies in a variety of populations revealed that some initially described disease-causing mutations are also found in normal individuals (22). This indicates that *OPTINEURIN* causes POAG when in permissive backgrounds, and acts as a key modifier in others (1). In cultured cells, OPTINEURIN can act to regulate apoptosis through interactions with tumor necrosis factor-alpha, but it is unknown how this occurs and whether this contributes to the apoptotic RGC cell loss found in POAG (23–26).

WDR36 encodes a protein of unknown function that was recently described as a causative gene for adult-onset POAG (27). Studies mapping POAG loci in affected families identified and narrowed a genetic linkage to 5q22.1 (GLC1G) (27–29). In one of these families, a coding variation in *WDR36* was found to segregate with all affected family members and not with any unaffected individuals (27). Further analysis of 17 unrelated patients with either high- or low-tension POAG revealed a total of four amino acid changes that were not found in 200 control individuals (27). When other groups extended the study of *WDR36* to different populations, the relationship between *WDR36* and glaucoma appeared more complex. Originally described disease-causing variants have been found in control individuals with an equal frequency as patients with POAG (30–33). Although these data indicate that *WDR36* is not causative for POAG in all populations, recent studies suggest that *WDR36* may act as a modifier of the disease. Hauser *et al*. (30) found correlations between *WDR36* variants and POAG severity in POAG pedigrees. Additional genetic association studies have also found a higher frequency of rare *WDR36* variants in glaucoma patients compared with controls, and have suggested that *WDR36* variants may contribute to a small number of unrelated glaucoma cases (32,34,35). Taken together, the current genetic data suggest that *WDR36* may act as a modifier of POAG, and/or as a causative gene for POAG in certain populations. Alternatively, *WDR36* variants may simply mark certain disease haplotypes and not be directly involved in POAG pathology. To better understand the role of *WDR36* in POAG, determining its function and manipulating the gene in animal models are crucial. Although the function of WDR36 is unclear, it is known that it is a 100 kDa protein containing four conserved protein domains: a guanine nucleotide-binding protein (G-beta) WD40 repeat, an AMP-dependant synthetase and ligase, a cytochrome cd1—nitrite reductase-like domain and a putative Utp21-specific WD40-associated domain (27). In human and mouse tissues, *WDR36* is widely expressed, and it was also found to be upregulated during human T-cell proliferation (27,36).

In this study, we use zebrafish to determine the function of Wdr36, the homolog of human WDR36, and investigate the affected cellular signaling pathways for its involvement in POAG. We show that Wdr36 is functionally homologous to the yeast Utp21, a component of the rRNA processome, and is involved in 18S rRNA processing and nucleolar homeostasis. We further show that *wdr36* loss of function results in activation of the p53 stress–response pathway, consistent with disrupted nucleolar function.

RESULTS

WDR36 shares sequence homology to yeast Utp21

To gain insight into the cellular function of vertebrate WDR36, BLASTp analysis using human WDR36 was carried out against *Drosophila melanogaster* (Dm), *Caenorhabditis elegans* (Ce) and *Sacchaormyces cerevisiae* (Sc)—organisms with extensive protein function data. The closest related proteins in each species were: *Dm*, AAK93538 (NP_650284); *Ce*, Y45F10D.7 (NP_502661); *Sc*, Utp21 (NP_013513) (37,38). Of the homologous proteins identified, only the putative yeast ortholog, Utp21, was studied. It was found that this protein is part of the yeast rRNA small-subunit (SSU) processome and is essential for 18S rRNA maturation (38,39). Human WDR36 shares 24% identity with yeast Utp21. Subsequent protein alignments revealed that Utp21 and zebrafish Wdr36 share 25% identity, whereas human WDR36 and zebrafish Wdr36 share 64% identity. To test the hypothesis that vertebrate Wdr36 is the functional homolog of yeast Utp21, we explored the expression and cellular consequences of loss of Wdr36 function in zebrafish.

wdr36 is ubiquitously expressed

The expression of *wdr36* was examined by RT–PCR and *in situ* hybridization. Similar to that reported for human and mouse, RT–PCR analysis suggested that zebrafish *wdr36* is ubiquitous as transcripts were detected in all embryonic and adult tissues assayed (Fig. 1) (27). It also indicated that *wdr36* is maternally contributed (Fig. 1). Zebrafish embryos do not begin zygotic transcription until the 512-cell stage, and instead rely on a large supply of maternal protein and transcripts for early development. Ubiquitous *wdr36* expression was also shown by *in situ* hybridization when the alkaline phosphatase reporter reaction was allowed to develop for longer periods of time (data not shown). Interestingly, shorter reporter reaction times showed enrichment of *wdr36* transcripts within tissues undergoing high levels of proliferation (Fig. 1). Tissues with the greatest levels included the developing eye cup, proliferative zones within the CNS and cells throughout the gut (Fig. 1). Within the eye, as differentiation progressed, high levels of gene expression were maintained in the lens and retinal periphery where growth is ongoing. These results indicate that *wdr36* is ubiquitously expressed, but is enriched in proliferative cells during development.

Wdr36 fusion proteins localize to the nucleolus and cytoplasm

To investigate the sub-cellular localization of Wdr36, we expressed various epitope-tagged versions of Wdr36 within multiple cell types in zebrafish embryos. Fusion protein expression was driven by an inducible heat shock promoter (*hsp70*) in an attempt to control the protein levels. Following heat shock induction, epitope-tagged Wdr36 localized to both the cytoplasm and nucleoli (Fig. 2). Multiple epitope tags (N- and C-terminus 6X-myc or YFP) all showed equivalent localizations. Nucleolar localization was confirmed by co-expressing with either Histone2A fusions, which localize to chromatin but not the nucleolus, or with B23, which specifically labels

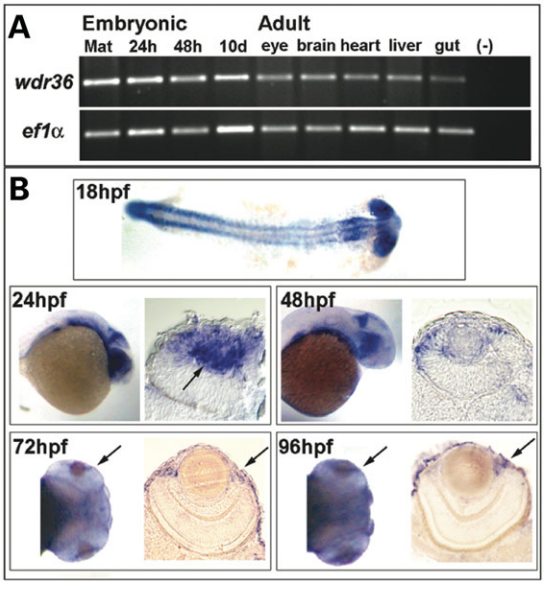

Figure 1. Expression of *wdr36*. (**A**) Expression analysis by RT–PCR showed *wdr36* transcript was present at all embryonic stages and in all adult tissues analyzed, including maternal (Mat) contributions. (**B**) By *in situ* hybridization, highly proliferative tissues showed enrichment of *wdr36*. At 18 hpf, enriched expression was found in the eye, CNS and somites. At 24 hpf, intense expression localized to the eye, the midbrain–hindbrain boundary in the CNS and the gut. Thin sections of the eye showed high levels of expression in the developing lens (arrow) and ciliary marginal zone (CMZ). Enriched expression continued to become restricted at 48 hpf. In ocular tissue at 72 and 96 hpf, enriched expression is localized to the CMZ (arrows).

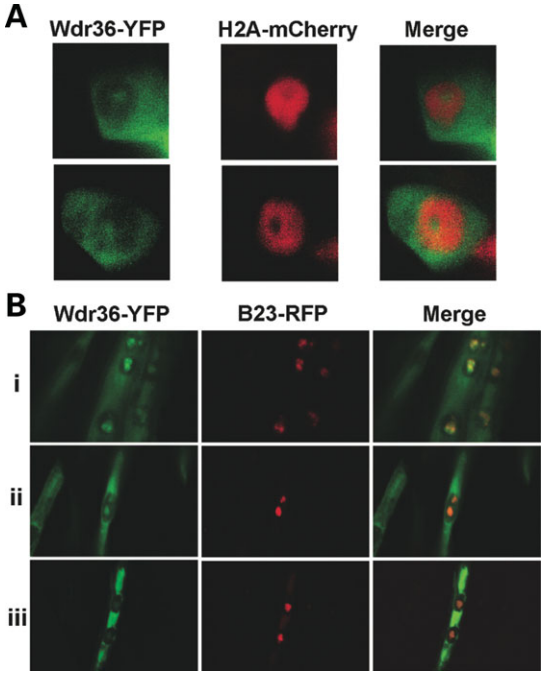

Figure 2. Sub-cellular localization of Wdr36. (**A**) Expression of Wdr36-YFP and Histone2A-mCherry indicated localization of Wdr36–YFP to the cytoplasm and a sub-nuclear structure void of chromatin. (**B**) Three co-expression examples (i–iii) of Wdr36-YFP and B23-RFP, a nucleolar marker. Co-localization of Wdr36-YFP and B23-RFP was found within the nucleolus. Variable levels of cytoplasmic and nucleolar Wdr36-YFP expression were observed.

the nucleolus (Fig. 2). In general, Wrd36 fusions first localized to nucleoli and then, as protein levels rose, became more enriched in the cytoplasm.

Wdr36 loss-of-function

To study the function of Wdr36 *in vivo*, a zebrafish line with a viral insert in the *wdr36* gene was utilized (*wdr36*^{hi3630aTg}). This recessive mutant was identified in a forward genetic screen for essential genes (40). The viral insert in the *wdr36* mutant was found within the first exon, about 40 nucleotide basepairs upstream of the start codon (Fig. 3A). Embryos heterozygous for the insert showed no phenotypic differences from wild-type (WT) siblings during development in any assays performed. Homozygous viral insert mutants (*wdr36* mutants) showed a reduction in *wdr36* transcript, but not a total loss, as assessed by semi-quantitative RT–PCR (Fig. 3B). We were not able to determine protein levels as our attempts to generate specific antibodies failed. *wdr36* mutants do not show visible phenotypes until ~3.5 days post-fertilization (dpf) at which point affected embryos are characterized by smaller heads and eyes. These phenotypes progress during development and by 6 dpf the small head and eye phenotypes are obvious compared with WT siblings (Fig. 3C). The other profound ocular phenotype is a lens opacity that presents with variable penetrance (Fig. 3C). Additionally, an obvious gut phenotype, including liver necrosis and absence of swim bladder inflation, develops by 6 dpf (Fig. 3C). Histological analysis of the eye at 5 dpf showed only subtle phenotypes. Although cellular differentiation and lamination of the retina appeared normal, a thickening of the lens epithelium was found and presumably accounts for the lens opacity. The proliferative margin of the retina also appeared to be reduced in the *wdr36* mutant embryos. Other than these subtle defects and smaller size, no other ocular abnormalities were found. Consistent with gross inspection of the embryo, histology of gut structures showed severe differentiation defects in the liver, pancreas and intestine (Fig. 6A, data not shown). All phenotypes progressively worsen and the embryos die by 11 dpf. Lethality is most likely due to defects in the gut organs. At 10 dpf, the eyes of mutants are very small compared with WTs, and a pin-hole pupil is present. Histology revealed progressive and severe lens degeneration, accounting for the dysmorphic pupil (Fig. 3D). Additionally, at this late stage of pathogenesis, the retina showed signs of degeneration, with thinning of all retinal layers and presence of dying cells with pyknotic nuclei (Fig. 3D).

To confirm the specificity of the phenotypes observed in the *wdr36* mutant embryos and to provide additional tools for analysis, antisense morpholinos (MOs) were designed against *wdr36*. Two non-overlapping MOs were designed; one targeting the start ATG codon to disrupt translation and one targeting the junction of exon 2:intron 2 to disrupt splicing. Both MOs gave identical phenotypes, and RT–PCR indicated that splicing of *wdr36* was disrupted by the second MO (Fig. 4A). Morphant embryos were also very similar to *wdr36* genetic mutants, confirming that the collective phenotypes result from loss of *wdr36* (Fig. 4B). The only clear difference observed between *wrd36* morphants and *wdr36* mutants was

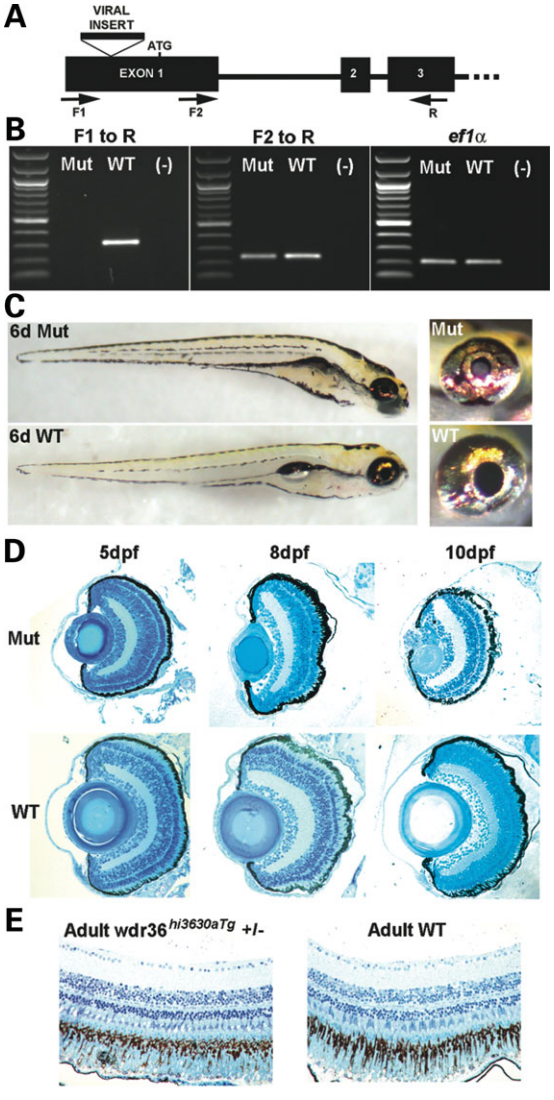

Figure 3. *wdr36* viral insert mutant phenotypes. (**A**) Schematic of the first three exons of *wdr36* showing location of viral insert, start codon and primers used to assess transcript. (**B**) Analysis of *wdr36* transcript in mutants by RT–PCR. Complete loss of transcript was found when amplifying across the viral insert (primers F1-R). Transcripts were still present when amplifying downstream of insert (F2-R), but levels were reduced. *ef1α* was used as a loading control. (**C**) Gross phenotype of 6 dpf *wdr36* mutants and WT siblings. Small head and eye phenotypes were found, along with defects in gut development. Note the absence of an inflated swim bladder. Lens opacity was also observed with incident light illumination of the eye. (**D**) Histological examination of the eye during development. At 5 dpf, *wdr36* mutant eyes were small but look grossly normal. Only a slight thickening of the lens epithelium and a reduced ciliary margin zone (CMZ) were observed. Mutant phenotypes progress during development, and at 8 dpf clear defects in the lens and CMZ remained. By 10 dpf, mutant larva showed severe lens degeneration and thinning of the retina, along with cells containing pyknotic nuclei. (**E**) Representative histological sections from 6--month-old heterozygous *wdr36*–insert and WT sibling fish. No gross differences between the two conditions are observed.

that the phenotypes showed slightly earlier in development when using MOs. With ATG MO injection, the small eye and head phenotypes were detected by 36 hpf. At 48 hpf, a delay in retinal lamination was observed by histology, along with phenotypes similar to *wdr36* mutant embryos (Fig. 4C).

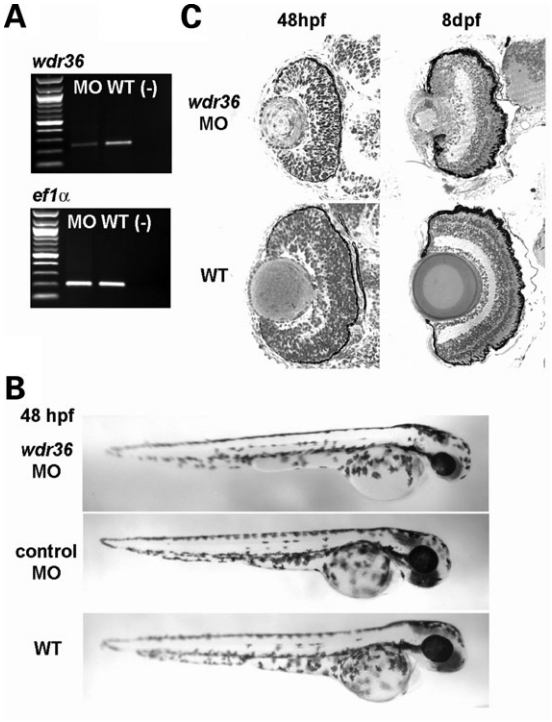

Figure 4. *wdr36* morphant phenotypes. (**A**) RT–PCR analysis comparing *wdr36* transcript from *wdr36* morphants and WT embryos. Reduced amounts of transcript are found following injection of the splice blocking MO. (**B**) Gross phenotypes of *wdr36* morphants compared with control morphants and WT embryos at 48 hpf. A small head and eye phenotype were observed, similar to *wdr36* mutants. (**C**) Histological analysis at 48 hpf revealed a delay in lamination. Like in the mutant, phenotypes were also progressive, as shown by the lens degeneration observed at 8 dpf in the *wdr36* morphant.

For example, the later onset lens degeneration was also observed at 8 dpf in *wdr36* morphants (Fig. 4C).

The *WDR36* variants associated with disease are inherited in a heterozygous manner, opening the possibility that disease may be caused by haploinsufficiency (27,30). To begin to address this possibility, we characterized eyes from adult heterozygous *wdr36*–insert fish. Overall appearance of heterozygous eyes, or the fish in general, did not differ from WT. Similarly, there were no changes in retinal histology between adult heterozygotes versus WT eyes (Fig. 3E). To explore whether more subtle defects occurred in the eyes of *wdr36*–insert heterozygotes, we measured *gap43* and *c1q* levels by real-time RT–PCR. Transcription of *gap43* is upregulated in zebrafish RGCs following axotomy or optic nerve crush, and *c1qc* is upregulated in optic neuropathies including glaucoma (41–44). Both genes were found to be expressed at low levels and no change in expression was found between *wdr36*–insert heterozygote and WT eyes for either gene (data not shown). Finally, no indications of increased IOP were noted in *wdr36*–insert heterozygotes, as judged by measuring corneal thickness and eye size to body length ratio, which can be affected with changes in IOP.

Defects in 18S rRNA processing with loss of *wdr36*

To test whether *wdr36* is functionally homologous to yeast *utp21*, we investigated the processing of 18S rRNA following

loss of Wdr36. rRNA is transcribed as a large 35S pre-rRNA transcript. The transcript undergoes a series of enzymatic cleavages within the nucleolus by large nucleo-protein complexes resulting in mature 18S, 5.8S and 25S rRNAs (45). 18S rRNA is utilized for the production of the small ribosomal subunit, and 5.8S and 25S rRNAs are used for the large subunit. The first cleavage steps in 35S rRNA processing separate the immature 18S rRNA from the 5.8 and 25S rRNAs. Distinct processomes for large and small subunit rRNAs then complete the maturation steps. The SSU processome, of which Utp21 is a part, is required specifically for small subunit (18S rRNA) maturation. After production in the nucleolus, mature subunits are transported to the cytoplasm where they are utilized for ribosome assembly. This process has been well studied in yeast, but in vertebrates the exact order of cleavage events has been found to vary across species. An outline of 18S maturation in the zebrafish is shown in Figure 5A (46). Northern blot analysis, using a probe against 18S rRNA, was carried out to investigate rRNA processing in *wdr36* mutants and morphants. This probe recognizes both the mature and immature transcripts, as well as the intermediate forms of 18S rRNA. The presence of the precursor, intermediate and mature forms was observed in WT controls (Fig. 5B). In contrast, high levels of the immature forms of 18S rRNA was observed in *wdr36* mutant and morphant embryos, but products from later maturation steps and the mature 18S rRNA were greatly reduced (Fig. 5B). This result shows a defect at one or more steps in the maturation of 18S rRNA following loss of *wdr36*, consistent with Wdr36 being the functional homolog of Utp21.

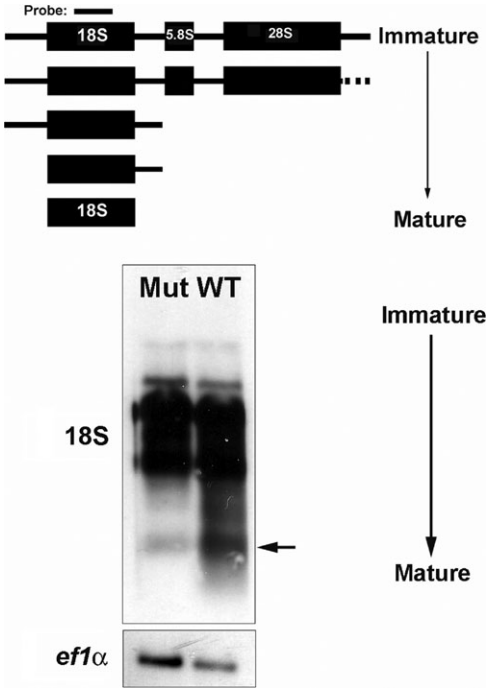

Figure 5. 18S rRNA processing in *wdr36* mutants. (**A**) Model of 18S rRNA processing in zebrafish and location of the probe used for the northern blot. (**B**) Representative northern blot of 18S rRNA processing in 6 dpf *wdr36* mutants and WTs. In WT, all products from immature to mature (arrow) are found. In contrast, only larger, immature transcripts were recovered from mutant embryos. A probe-recognizing *ef1α* was used as a loading control.

Nucleolar morphology is disrupted with loss of *wdr36*

To address whether the observed defects in 18S rRNA processing had an effect on the nucleolus, histological sections of retinal neurons, intestinal epithelia and liver cells from *wdr36* mutants and morphants were analyzed at high magnifications. In these tissues, the nucleolus appeared large and dysmorphic with loss of Wdr36 compared with controls (Fig. 6A). To confirm these findings, nucleolar morphology was analyzed by transmission electron microscopy. Again, Wdr36-deficient nucleoli were enlarged, dysmorphic and often less electron dense compared with WT control cells (Fig. 6B).

Loss of *wdr36* results in activation of the p53 stress–response pathway

It is well documented that disruption of nucleolar morphology and ribosome biogenesis results in activation of the p53 stress–response pathway (47). When the nucleolus is disrupted, activated ADP-ribosylating factors (Arfs) and free ribosomal proteins are released from the nucleus into the cytoplasm. Once in the cytoplasm, these proteins interact with Mdm2. The normal function of Mdm2 is to bind, ubiquinate and maintain p53 in an inactive state. When Mdm2 interacts with free nucleolar proteins released following disruption of the nucleolus, Mdm2 no longer inhibits p53. The resultant activation of p53 can then promote transcription of itself along with pro-apoptotic and/or cell cycle arrest genes. To address whether a p53 stress–response was activated with loss of *wdr36*, we first investigated whether expression of *p53* and its target genes were altered following loss of Wdr36. Semi-quantitative and real-time quantitative RT–PCR showed that while *p53* transcripts were present, the levels were not different between control and Wdr36-deficient embryos (Fig. 7A and B). However, a truncated isoform of *p53*, Δ113*p53*, was significantly upregulated in *wdr36* mutants and morphants as shown by semi-quantitative and quantitative RT–PCR (Fig. 7A and B). The Δ113*p53* isoform results from an alternate start site in the fourth intron and lacks part of the DNA-binding domain (48,49). The corresponding human isoform, Δ133*p53*, causes upregulation of cell cycle arrest genes but acts in a dominant-negative fashion to block induction of pro-apoptotic transcripts (49). This was previously confirmed in the zebrafish *def* mutant, which displays hypoplastic digestive organs (48). In *def* mutants, markers of cell cycle arrest were transcriptionally upregulated, but markers of apoptosis were not. We found similar results after loss of Wdr36. The cyclin-dependent kinase inhibitor *p21* was significantly upregulated, whereas the pro-apoptotic gene *bax* was not altered with the onset of Wdr36-deficient phenotypes (Fig. 7A). Overall, these experiments suggest that the p53 stress–response pathway is activated with loss of *wdr36*.

To probe these effects deeper, we analyzed apoptosis directly by scoring pyknotic nuclei and the expression of activated caspase-3 immunoreactivity. No change in either indicator of apoptosis was found at the onset of overt phenotypes (data not shown). At 10 dpf, in concordance with the observed trend toward an increase in p53, evidence

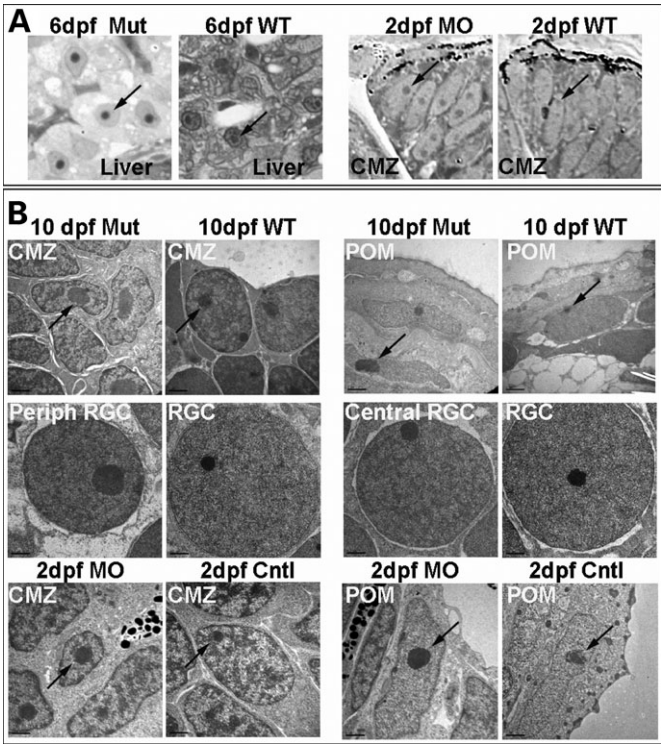

Figure 6. Nucleolar morphology following loss of Wdr36. (**A**) Light microscopy of liver cells from 6 dpf *wdr36* mutants and WTs, and CMZ cells from 2 dpf *wdr36* morphants and WTs. Note that with loss of Wdr36, nucleoli were larger, less in number per cell and were more centrally located compared with WT controls. (**B**) TEM images of nucleoli (arrows) from multiple cell types after loss of Wdr36 versus controls. Within the peripheral retina, mutant nucleoli in retinal ganglion cells were large and dysmorphic, while mutant nucleoli from the central retina were more normal in appearance. CMZ, ciliary marginal zone; POM, periocular mesenchyme; RGC, retinal ganglion cell.

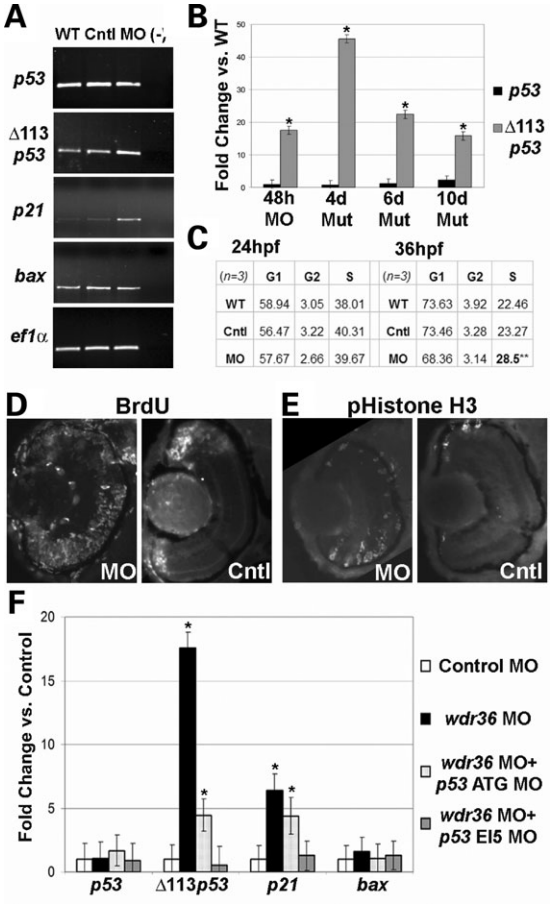

Figure 7. Activation of the p53 stress–response pathway with loss of Wdr36. (**A**) Semi-quantitative RT–PCR analysis of *p53*, Δ113*p53, p21* and *bax* in 48 hpf *wdr36* morphants versus control morphants and WTs. No changes were found in the levels of *p53* or *bax* transcripts. Increased transcript levels were observed for both Δ113*p53* and *p21. ef1α* was used as a loading control. (**B**) Quantitative RT–PCR analysis of *p53* and Δ113*p53* transcript levels in *wdr36* mutants and morphants at specified ages. Moderately increased *p53* levels were found only in 10 dpf *wdr36* mutants. Increased Δ113*p53* levels were found in both mutants and morphants at all ages assayed. Error bars show standard error of the mean ($^*P < 0.02$ versus control, Student's *t*-test). (**C**) FACS analysis of cell cycle phases after Wdr36 loss. No change in the cell cycle was found at 24 hpf. At 36 hpf, *wdr36* morphants showed a significant increase in the percentage of cells in S-phase. ($P < 0.03$; Students *t*-test). (**D**) BrdU labeling of cells in S-phase after a 10 h pulse from 48 to 58 hpf. In control embryos, proliferating cells were limited to the CMZ, while in the *wdr36* morphants more proliferating cells were present overall and were located throughout the retina. (**E**) phospho-Histone H3 staining of cells in M-phase. Proliferating cells in controls were localized to the CMZ, while more immunoreactive cells were found and were located across the retina in the *wdr36* morphants. (**F**) Quantitative RT–PCR analysis *of p53*, Δ113*p53, p21* and *bax* in 48 hpf *wdr36* morphants +/− p53 MOs versus control morphants. No changes in *p53* or *bax* transcript levels were found in any condition. The levels of both Δ113*p53* and *p21* transcript levels were increased in *wdr36* morphants, but this increase was partially rescued by co-injection of p53 ATG MO and fully rescued with co-injection of p53 EI5 MO. Error bars show standard error of the mean ($^*P < 0.02$ versus control, Student's *t*-test).

of apoptosis was found by both measures (data not shown). In contrast, defects in cell cycle regulation were found in *wdr36* MOs at the onset of overt phenotypes. Propidium iodide fluorescent-activated cell sorting (FACS) (DNA content), BrdU labeling (S-phase) and phospho-Histone H3 [late G2/M-phase] analyses were used to probe changes in the cell cycle. At 36 hpf, FACS analysis showed that Wdr36-deficient embryos had disproportionately greater percentage of cells in S-phase (Fig. 7C). Furthermore, long-pulse BrdU-labeling confirmed the FACS results and suggested that in addition to changes in cell cycle kinetics, cell cycle exit was also delayed within the retina. Altered cell cycle exit was indicated by the presence of proliferating cells in the *wdr36* morphant central retina at 58 hpf (Fig. 7D). At this time in WT retinas, proliferation was restricted to the ciliary marginal zone (CMZ; Fig. 7D). A delay in cell cycle withdrawal was confirmed by observing increased M-phase cells by phospho-Histone H3 analysis (Fig. 7E).

Finally, to address the dependence of these stress responses on p53 function, we measured *p53*, Δ113*p53*, *p21*, and *bax* expression by quantitative RT-PCR in *wdr36* morphants that also were depleted of either p53 isoform. This was accomplished by co-injecting one-cell stage embryos with *wdr36* MO and one of two previously described *p53* MOs; one that targets the ATG start codon (p53 ATG MO), which will only disrupt the translation of full-length p53 protein, and a second splice-disrupting MO targeting the intron 4–exon 5 boundary (p53EI5), which will affect both full-length and Δ113p53 proteins (48,50). In these experiments, we found

that the induction of both Δ113*p53* and *p21* caused by loss of Wdr36 was dependent on p53 function. Knockdown of full-length p53 alone partially rescued these stress–response genes to control levels, while co-depletion of both p53 isoforms completely prevented their induction (Fig. 7F).

DISCUSSION

In this study, a function for the POAG gene identified at locus GLC1G, *WDR36*, was determined. This is the first POAG gene currently identified for which a clear function has been described. The two previously discovered genes, *MYOCILIN* and *OPTINEURIN*, have both been extensively studied, but no endogenous function has yet been determined.

Wdr36 functions in 18S rRNA processing

We have provided evidence that WDR36 functions in the processing of 18S rRNA. BLAST studies and protein alignments have shown that WDR36 is structurally homologous to yeast Utp21, which is part of the SSU processome. In yeast, this processome is essential for the maturation of 18S rRNA, and thus ribosome biogenesis (39). Evidence for Wdr36 as the functional homolog of Utp21 comes from data showing tissue distribution, sub-cellular localization and loss-of-function phenotypes.

Ribosome biogenesis is an essential process, so ubiquitous expression of 18S rRNA processing genes is expected. Previous evidence of widespread expression in mouse and human tissues (27), along with data presented here of expression patterns by both RT–PCR and *in situ* hybridization, shows that *wdr36* is ubiquitously expressed. Further, enrichment in highly proliferative tissues was observed, consistent with an increased demand for ribosome biogenesis in proliferating cells.

At the sub-cellular level, Utp21 is localized to the nucleolus, the site of rRNA processing in the cell (38). Fusion proteins showed that Wdr36 also localizes to the nucleolus in vertebrate cells. YFP-tagged Wdr36 was found in this sub-compartment of the nucleus, as demonstrated by co-expression studies with the chromatin maker Histone2A, and a known nucleolar component, B23. Supporting these findings, mass spectrometry analysis of nucleoli isolated from cultured human cells showed WDR36 to be a component of this structure (http://www.lamondlab.com/NOPdb/) (51). Along with nucleolar localization, the epitope-tagged Wdr36 fusion proteins also showed strong cytoplasmic expression. Potentially, this may be a consequence of over-expression or epitope tagging. Alternatively, endogenous Wdr36 may also reside within the cytoplasm, similar to other nucleolar proteins (52).

Overall, our studies also do not rule out the possibility of additional functions for Wdr36. Some nucleolar proteins are known to have functions outside of ribosome biogenesis and these proteins also localize in the cytoplasm (47). For example, there is evidence that nucleolar components can directly influence the cell cycle and that proteins such as B23 and rRNA processing factors, re-localize to structures within the cytoplasm during mitosis (47).

The loss-of-function phenotypes described in this study provide evidence that Wdr36 is the functional homolog of Utp21. A *wdr36* viral insert mutant shows defects in highly proliferative tissues; the eye, CNS and gut. These defects are consistent with the enriched expression in proliferating tissues observed by *in situ* hybridization and a higher need for ribosome biogenesis with cell expansion. MO knockdown of Wdr36 shows equivalent phenotypes as the mutants, confirming that these defects are due to loss of Wdr36. Informatively, both mutants and morphants showed disrupted 18S rRNA processing. Northern blot analysis indicated a strong reduction in processed 18S rRNA products and accumulation of larger immature pre-RNAs. In addition, both *wdr36* mutant and morphant embryos show disrupted nucleolar morphology. These data suggest that the accumulation of unprocessed rRNAs within the nucleolus causes the enlarged nucleolar phenotype.

The results we have presented here are consistent with WDR36 being the functional homolog of Utp21, a component of the SSU processome and a protein involved in 18S rRNA processing. While an essential role for human WDR36 in rRNA processing is implicated by our experiments, the exact function that WDR36 plays within the processome is not clear. WDR36 contains nine WD40 repeat domains, which commonly facilitate protein–protein interactions. WDR36 may be necessary for structural integrity of the processome complex and/or have a necessary enzymatic function. The yeast work done to date on Utp21 does not offer any further insight. Utp21 was identified as part of the SSU processome by showing physical interaction with components of the complex, but its specific function was not probed (38).

It is surprising that disrupting a component of such a cell essential process does not result in earlier, more severe phenotypes. The maternal expression of *wdr36* provides one possibility for the mild early phenotypes. WT *wdr36* transcripts and perhaps protein derived from the WT allele of the *wdr36* heterozygotic parent likely enables the mutant embryo to survive early development. It is not until after the WT maternal supplies are lost by degradation or diluted during cell divisions that phenotypes can be observed. This interpretation is suggested from observations within the developing retina, where earlier-born cells within the central retina show a more normal nucleolar morphology than later-born neurons at the periphery or in actively proliferating cells of the ciliary margin. This also explains the observed earlier phenotypes found with the ATG MO, which will block translation of both maternal and zygotic mRNA, although it still will not affect maternal protein.

Activation of the p53 stress–response pathway after loss of Wdr36

Activation of the p53 stress–response pathway after disruptions in nucleolar morphology is well documented (47). We show that in *wdr36* mutants and morphants, the p53 stress–response pathway is also activated. With loss of Wdr36 during embryogenesis, the disruption in nucleolar homeostasis results in significant upregulation of the truncated form of p53, Δ113p53. It has previously been reported that this isoform results in an arrest of the cell cycle, and may also act to

block p53-mediated apoptosis (48,49). Consistently, the loss of Wdr36 initially results in delayed cell cycle progression, without cell death. This response, versus one including apoptosis, may be advantageous during development by giving embryos a chance to recover from a transient stress. With loss of Wdr36, however, stress caused by nucleolar defects is not transient, and the classic p53 stress–response, including apoptosis, appears to occur. Evidence for a direct role of the p53 stress pathways in gene expression caused by Wdr36 deficiencies was found by blocking p53 using MOs. While complete molecular recovery of the phenotypes was found, the gross appearance of the *wdr36* morphant embryos was not significantly affected by co-injection of either p53 MO. To address whether maternal stores of p53 protein—which would not be affected by the MOs—were preventing phenotype rescue, *wdr36* MO was also injected into embryos from an incross of $p53^{M214K/M214K}$ zebrafish (53). These fish are homozygous for a non-functional p53 allele and are thus not able to maternally contribute WT p53. Again, no change in phenotype versus WT embryos injected with *wdr36* MO was noted. Together, this suggests that either alternate stress pathways are activated, or simply the inability to establish functional protein translation machinery itself causes the observed gross phenotypes.

Wdr36 and disease

The evidence that we have presented, that WDR36 is important for 18S rRNA processing, leads to the question whether *WDR36* is the POAG causative (or modifying) gene at locus GLC1G? The possibility of a gene encoding an essential and ubiquitous protein, yet underlying a very specific pathogenesis-like POAG, is surprising, but is not without precedence. For example, four pre-mRNA splicing factors have recently been identified as causative for certain types of autosomal dominant retinitis pigmentosa (RP), another retina-specific blinding disorder in humans (54–57). In addition, mutations in essential nucleolar, 18S rRNA processing genes, such as RPS19 and dyskerin, have been shown to cause tissue-specific human disease (58–60). If *WDR36* does play a role in POAG, it likely occurs in a permissive genetic context, much like the case with *OPTENEURIN*. This is not surprising given the complex nature of POAG. In line with this possibility, we have shown that Wdr36 interacts with p53; a key regulator of the apoptotic pathway. In POAG, it is established that RGCs are lost because of apoptosis (61,62). Genetic studies have been conducted to assess whether a direct relationship between p53 genetic variants and POAG exists, but, like other genes implicated in POAG, different studies have yielded somewhat contradictory results (63–66). Our data showing an interaction of p53 and WDR36 suggest that variants in these genes could potentially synergize in POAG pathogenesis. It may be that genetic changes in each gene alone do not cause disease, but when co-inherited, RGCs are at a higher risk for apoptosis, particularly when stressed by elevated IOP or other factors. Consistent with this concept, WDR36 has already been suggested to affect the severity of *MYOCILIN*-based disease (30). Overall, the functional evidence we have presented lays essential groundwork to address these issues, but does not answer whether *WDR36* is involved in POAG. Genetic studies have shown that associated variants are present in a heterozygous state, suggesting disease may be caused by haploinsufficiency, dominant negative activities or possibly through a gain of function mechanism (27,30). Our initial results with heterozygous *wdr36* mutants suggest that haploinsufficiency of *WDR36* alone is not sufficient for disease. Further studies determining the effects of disease-associated variants on the normal function of WDR36 will be necessary to address how and if WDR36 may influence POAG.

In conclusion, we have shown that WDR36 functions in 18S rRNA processing. Loss of Wdr36 in zebrafish leads to proliferation defects in the eye and other tissues, as well as severe dysgenesis of lens. At the cellular level, loss of Wdr36 disrupts 18S rRNA maturation and leads to nucleolar morphology defects resulting in activation of the p53 stress–response pathway. The results from this study provide basis for further research to determine whether *WDR36* variants are in fact involved in POAG.

MATERIALS AND METHODS

Whole-mount *in situ* hybridization

A 563 bp fragment of the zebrafish *wdr36* gene was amplified by PCR with the following primers: F: 5′-TGCAGACTA TGAGCCGACTG-3′ and R: 5′-*TAATACGACTCACTATAGG GCGA*CTTGGGCCAGGTCAAAATCT-3′. The R primer includes a T7 RNA polymerase promoter (shown in italics). This PCR product was used as a template for cRNA probe generation. cRNA probes were produced and whole-mount *in situ* hybridization was conducted as described previously (67,68). Ten to fifteen embryos, treated with 0.003% phenylthiourea (PTU), were analyzed in each *in situ* experiment, PTU inhibits melanin synthesis. For post-hybridization sectioning, embryos were fixed in 4% paraformaldehyde/PBS and infiltrated with 15% sucrose, 30% sucrose and then 100% Tissue-Tek OCT (Miles Inc., Elkhart, IN, USA). Embryos were oriented in a freezing mold and 10 μm sections were cut on a cryostat and mounted on gelatin-coated glass slides.

Quantitative and semi-quantitative RT–PCR

Total RNA was extracted from either single zebrafish embryos using 100 μl TRIZOL reagent (Invitrogen, Carlsbad, CA, USA) and 1 μl 10 mM glycogen (Roche, Indianapolis, IN, USA) or from pools of 10–50 embryos using the RNeasy Plus Mini Kit (Qiagen, Valencia, CA, USA). cDNA was produced using 0.25–1.0 μg of RNA with the SuperScript III Reverse Transcriptase enzyme (Invitrogen). Semi-quantitative PCR was done using Amplitaq Gold (Roche). qPCRs were carried out using the iQ SYBR Green Supermix (Bio-Rad, Hercules, CA, USA) on the iCycler iQ Real-Time Detection System (Bio-Rad). At least three-independent cDNA samples were assayed in triplicate for each primer set. *ef1α* was used for normalization. Data were analyzed using the ΔΔCt method (69). Primers are listed in Table 1.

Table 1. Primer, construct and morpholino details

Gene (gene ID)	Primer name	Seq: 5′–3′	Product size (bp)	Ref.
Semi- and qRT–PCR primers				
wdr36 (321745)	*wdr36 F1*	TGTTTTGCTACTGTTCTCTGCTG	308	This study
	wdr36 R	GGCATTACTGACTGCAACGA		This study
	wdr 36 F2 (with wdr36 R)	TGAGCACAGACAGCGAAGAT	240	This study
p53 (30590)	*p53 F*	CTCTCCCACCAACATCCACT	178	(70)
	p53 R	ACGTCCACCACCATTTGAAC		(70)
	Δ*113p53 F* (use with p53 R)	ATATCCTGGCGAACATTTGG	214	(70)
p21 (AL912410)	*p21 F*	GAAGCGCAAACAGACCAACAT		(42)
	p21 R1 (semi-quant)	GCAGCTCAATTACGATAAAGA	544	(42)
	p21 R2 (qPCR)	CGGAATAAACGGTGTCGTCT	219	This study
bax (58081)	*bax F*	GGAGGCGATACGGGCAGTG		(42)
	bax R1 (semi-quant)	TTGCGAATCACCAATGCTGTG	534	(42)
	bax R2 (qPCR)	TCGGCTGAAGATTAGAGTTGTTT	250	This Study
ef1 α(30516)	*ef1α F*	TCTCTCAATCTTGAAACTTATCAATCA	205	This study
	elfα R	AACACCCAGGCGTACTTGAA	177	This study
c1qc (449803)	*c1qc F*	CTCTGCTGACACCTGTCCTG	170	This study
	c1qcR	GGTGGTCCTTTCAGACCAAA		This study
gap43 (30608)	*gap43 F*	CCTAACTCCCCAGCAAATGA		This study
	gap43 R	GCATTGCCTTCTTCTTCAGG		This study
Fusion protein primers				
wdr36	wdr36 GW F	GGGGACAAGTTTGTACAAAAAAGCAGGCTTCGAAGGAGGTAGAACC**ATG**AGCAGCATGTCTGCGA	2767	This study
	wdr36 GW R	GGGGACCACTTTGTACAAGAAAGCTGGGTACAGCAGCGCACTCTTGATA		This study
b23 (npm1) (266985)	B23 GW F	GGGGACAAGTTTGTACAAAAAAGCAGGCTTCACC**ATG**GATCTCGAACAGATGGG	909	This study
	B23 GW R	GGGGACCACTTTGTACAAGAAAGCTGGGTATTTGACAGTCTGTCTCCAC		This study
Both wdr36 and b23 were cloned into a gateway compatible destination vector containing 6X UAS with C-term epitope tags				This study
H2A-mCherry construct produced using the following clones from the Tol2kit: 5′ entry no. 234, 3′ entry no. 302 into destination clone no. 394				(67)
Morpholinos				
Name	Amount used/embryo	Seq: 5′–3′		**Ref.**
wdr36 ATG	4–8 ng	TCGCCAGCACAATCTTAATCTTCGC		This study
wdr36 exon2–intron 3	14 ng	GTACTGAATCCTACTTACTGACTGC		This study
p53 ATG	10 ng	GCGCCATTGCTTTGCAAGAATTG		(43)
p53 Exon-Intron 5	10 ng	AAAATGTCTGTACTATCTCCATCCG		(42)
Control	=to experimental MO	CCTCTTACCTCAGTTACAATTTATA		From gene tools

Generation of fusion proteins and sub-cellular localization

C-terminally tagged versions of Wdr36, B23 and H2A were generated using the Gateway Clonase II system (Invitrogen) and tol2-based vectors were modified for Gateway recombinations (70). Constructs were generated with primers and vectors found in Table 1. The final constructs were co-injected either with a plasmid containing Gal4 under the control of the *ef1α* promoter or into the HSP70–Gal4 transgenic zebrafish line. Constructs were injected into 1–4-cell embryos as described above. Injected HSP70–Gal4 tg embryos were subjected to a 30 min incubation at 37°C at 24 hpf to activate Gal4 expression and consequently the UAS promoter to drive fusion protein expression. Embryos were imaged from 24 to 48 hpf by confocal microscopy.

Transmission electron microscopy and histological analysis

Histological specimens for light microscopy were processed as described previously (71). In brief, embryos were fixed in primary fixative [2% paraformaldehyde, 2.5% glutaraldehyde, 3% sucrose, 0.06% phosphate buffer (pH 7.4)] at 4°C for 24 h and then washed in 0.1 M PBS, dehydrated through an ethanol series and propylene oxide and then infiltrated with EMbed-812/Araldyte resin mixture. Semi-thin plastic sections were cut with a glass knife on a JB4 microtome and stained with 1% toluidine blue in 1% borax. For transmission electron microscopy, an additional fixation in 1.0% osmium was included, followed by dehydration in MeOH/Aralhydrate. Embryos were then embedded in EMBed-812/DER 736. Ultrathin sections (60–70 nm) were collected on coated grids and stained with uranyl acetate and lead citrate for contrast. Images were captured using Hitachi H600 transmission electron microscopy.

Morpholino knockdown

Two MOs were designed against *wdr36*: one to block mRNA splicing and one to block translation. The *wdr36* MOs and previously described MOs against p53 isoforms were ordered from Gene Tools (Corvallis, OR, USA) (48,50). A list of MOs used is given in Table 1. MOs were resuspended in water and injected into one- to two-cell stage embryos using a Nanoject II injector (Drummond Scientific, Broomall,PA, USA).

Analysis of adult phenotypes

Both eyes from three adult *wdr36* heterozygous and three WT siblings were dissected and used for expression analysis by qRT–PCR as described earlier. Primers used are listed in Table 1. To determine the body length to eye ratio, the lengths of four adult fish from each group were measured from tip of mouth to beginning of the tail by ruler and eye size was determined using morphometric analysis (MetaMorph Software, Molecular Devices, Sunnyvale, CA, USA) of dorsal view images, using the same ruler for calibration. These measures were then divided to obtain the ratio of eye size: body length and groups were compared by Student's *t*-test. Corneal thickness was determined by using morphometric analysis (MetaMorph) to measure the width of corneas from histological sections of three eyes from each group. For each fish, five different sections were measured and averaged before comparison was made across fish. Groups were then compared by Student's *t*-test.

Northern blot analysis of rRNA processing

Total RNA was isolated as described earlier. One microgram of total RNA was separated on 1% agarose–formaldehyde gels and capillary transferred with 20× SSC onto positively charged nylon membranes (Roche). Blots were analyzed using the DIG Northern Starter Kit following the manufacturer's protocol (Roche). A plasmid previously described containing the 18S target sequence was generously provided by the Dawid Lab (NICHD, NIH) and used to make DIG-labeled probes against 18S rRNA (46). An 815 bp fragment of *ef1a* was PCR amplified, TA cloned into the pCRII-TOPO vector (Invitrogen) and used to make the DIG-labeled control probe. Probes were produced as per manufactures recommendation with 1 μg of linearized plasmid (Roche, DIG Northern Starter Kit). Primers to amplify *ef1α*: 5′-TGATCTACAAAT GCGGTGGA-3′; 5′-GAGACTCGTGGTGCATCTCA-3′.

FACS DNA CONTENT ANALYSIS

Cell cycle/DNA content was analyzed as described previously (72). Approximately 30–40 whole embryos at specified stages were pooled, washed with E3 solution (5 mM NaCl, 0.17 mM KCl, 0.33 mM $CaCl_2$, 0,33 mM $MgSO_4$), placed into DMEM+10% serum and disaggregated on ice. Cells were serially passed through 105 and 40 μm filters, washed with 1X PBS, stained with 0.05 mg/ml propidium iodide and RNase treated. Three pools of embryos for each condition and time point were assayed independently. FACS analysis was done on a FACS Calibur (Becton-Dickinson, San Jose, CA, USA) and analyzed using Modfit LT software (Verity Software House, Topsham, ME, USA).

ACKNOWLEDGEMENTS

We thank Michael Walter, PhD for informative and helpful discussions; Igor Dawid, PhD and Adam Amsterdam, PhD for reagents; Pat Cliff and Melissa Reske for technical support; the MCW Flow Cytometry Core Facility and Clive Wells, PhD of the MCW EM Core Facility.

Conflict of Interest statement. None declared.

FUNDING

National Institutes for Health (R01EY16060 to B.A.L., F30AG029763 to J.M.S., and T32 EY014537—Research Training Program in Vision Science to J.M.S.).

REFERENCES

1. Libby, R.T., Gould, D.B., Anderson, M.G. and John, S.W. (2005) Complex genetics of glaucoma susceptibility. *Annu. Rev. Genomics Hum. Genet.*, **6**, 15–44.
2. Quigley, H.A. (1996) Number of people with glaucoma worldwide. *Br. J. Ophthalmol.*, **80**, 389–393.
3. Fraser, S. (2004) Epidemiology of primary open angle glaucoma. In Hitchings, R. (ed.), *Glaucoma*. BMJ Publishers, London, pp. 9–15.
4. Kang, J.H., Pasquale, L.R., Willett, W.C., Rosner, B.A., Egan, K.M., Faberowski, N. and Hankinson, S.E. (2004) Dietary fat consumption and primary open-angle glaucoma. *Am. J. Clin. Nutr.*, **79**, 755–764.
5. Kang, J.H., Willett, W.C., Rosner, B.A., Hankinson, S.E. and Pasquale, L.R. (2008) Caffeine consumption and the risk of primary open-angle glaucoma: a prospective cohort study. *Invest. Ophthalmol. Vis. Sci.*, **49**, 1924–1931.
6. Flammer, J. and Mozaffarieh, M. (2007) What is the present pathogenetic concept of glaucomatous optic neuropathy? *Surv. Ophthalmol.*, **52** (Suppl. 2), S162–S173.
7. Neufeld, A.H. and Liu, B. (2003) Glaucomatous optic neuropathy: when glia misbehave. *Neuroscientist*, **9**, 485–495.
8. Quigley, H.A. (1995) Ganglion cell death in glaucoma: pathology recapitulates ontogeny. *Aust. N. Z. J. Ophthalmol.*, **23**, 85–91.
9. Howell, G.R., Libby, R.T., Jakobs, T.C., Smith, R.S., Phalan, F.C., Barter, J.W., Barbay, J.M., Marchant, J.K., Mahesh, N., Porciatti, V. *et al.* (2007) Axons of retinal ganglion cells are insulted in the optic nerve early in DBA/2J glaucoma. *J. Cell Biol.*, **179**, 1523–1537.
10. Chen, L., Yang, P. and Kijlstra, A. (2002) Distribution, markers, and functions of retinal microglia. *Ocul. Immunol. Inflamm.*, **10**, 27–39.
11. Nickells, R.W. (2007) From ocular hypertension to ganglion cell death: a theoretical sequence of events leading to glaucoma. *Can. J. Ophthalmol.*, **42**, 278–287.
12. Werner, E. (1996) Normal-tension glaucoma. In Ritch, R.S. and Krupin, M.T. (eds), *The Glaucomas*, 2nd edn. Mosby, St. Louis, Vol. **2**, pp. 769–797.
13. Fan, B.J., Wang, D.Y., Lam, D.S. and Pang, C.P. (2006) Gene mapping for primary open angle glaucoma. *Clin. Biochem.*, **39**, 249–258.
14. Stone, E.M., Fingert, J.H., Alward, W.L., Nguyen, T.D., Polansky, J.R., Sunden, S.L., Nishimura, D., Clark, A.F., Nystuen, A., Nichols, B.E. *et al.* (1997) Identification of a gene that causes primary open angle glaucoma. *Science*, **275**, 668–670.
15. Tamm, E.R. (2002) Myocilin and glaucoma: facts and ideas. *Prog. Retin. Eye Res.*, **21**, 395–428.
16. Liu, Y. and Vollrath, D. (2004) Reversal of mutant myocilin non-secretion and cell killing: implications for glaucoma. *Hum. Mol. Genet.*, **13**, 1193–1204.
17. Johnson, D.H. (2000) Myocilin and glaucoma: A TIGR by the tail? *Arch. Ophthalmol.*, **118**, 974–978.
18. Shepard, A.R., Jacobson, N., Millar, J.C., Pang, I.H., Steely, H.T., Searby, C.C., Sheffield, V.C., Stone, E.M. and Clark, A.F. (2007) Glaucoma-causing myocilin mutants require the peroxisomal targeting signal-1 receptor (PTS1R) to elevate intraocular pressure. *Hum. Mol. Genet.*, **16**, 609–617.
19. Gobeil, S., Letartre, L. and Raymond, V. (2006) Functional analysis of the glaucoma-causing TIGR/myocilin protein: integrity of amino-terminal coiled-coil regions and olfactomedin homology domain is essential for extracellular adhesion and secretion. *Exp. Eye Res.*, **82**, 1017–1029.
20. Jacobson, N., Andrews, M., Shepard, A.R., Nishimura, D., Searby, C., Fingert, J.H., Hageman, G., Mullins, R., Davidson, B.L., Kwon, Y.H. *et al.* (2001) Non-secretion of mutant proteins of the glaucoma gene myocilin in cultured trabecular meshwork cells and in aqueous humor. *Hum. Mol. Genet.*, **10**, 117–125.
21. Rezaie, T., Child, A., Hitchings, R., Brice, G., Miller, L., Coca-Prados, M., Heon, E., Krupin, T., Ritch, R., Kreutzer, D. *et al.* (2002) Adult-onset primary open-angle glaucoma caused by mutations in optineurin. *Science*, **295**, 1077–1079.
22. Alward, W.L., Kwon, Y.H., Kawase, K., Craig, J.E., Hayreh, S.S., Johnson, A.T., Khanna, C.L., Yamamoto, T., Mackey, D.A., Roos, B.R. *et al.* (2003) Evaluation of optineurin sequence variations in 1,048 patients with open-angle glaucoma. *Am. J. Ophthalmol.*, **136**, 904–910.
23. Rezaie, T., Waitzman, D.M., Seeman, J.L., Kaufman, P.L. and Sarfarazi, M. (2005) Molecular cloning and expression profiling of optineurin in the rhesus monkey. *Invest. Ophthalmol. Vis. Sci.*, **46**, 2404–2410.
24. Rezaie, T. and Sarfarazi, M. (2005) Molecular cloning, genomic structure, and protein characterization of mouse optineurin. *Genomics*, **85**, 131–138.
25. Sarfarazi, M. and Rezaie, T. (2003) Optineurin in primary open angle glaucoma. *Ophthalmol. Clin. North Am.*, **16**, 529–541.
26. Chen, P., Tian, J., Kovesdi, I. and Bruder, J.T. (1998) Interaction of the adenovirus 14.7-kDa protein with FLICE inhibits Fas ligand-induced apoptosis. *J. Biol. Chem.*, **273**, 5815–5820.
27. Monemi, S., Spaeth, G., DaSilva, A., Popinchalk, S., Ilitchev, E., Liebmann, J., Ritch, R., Heon, E., Crick, R.P., Child, A. *et al.* (2005) Identification of a novel adult-onset primary open-angle glaucoma (POAG) gene on 5q22.1. *Hum. Mol. Genet.*, **14**, 725–733.
28. Kramer, P.L., Samples, J.R., Schilling, K., Sykes, R.L., Man, J., Rust, K. and Wirtz, M.K. (2004) Mapping the GLC1G locus for primary open-angle glaucoma (POAG) in an Oregon family of Dutch origin. *Am. J. Hum. Genet.*, Vol. 75. Abstract #1914 presented at 2004 American Society for Human Genetics Annual Meeting in Toronto, Ontario, Canada.
29. Samples, J.R., Sykes, R., Man, J., Rust, K., Kramer, P.L. and Wirtz, M.K. (2004) Mapping a new POAG locus on chromosome 5. *The Association for Research in Vision and Ophthalmology (ARVO) annual meeting*, Fort Lauderdale, FL, Vol. Abstract no. 4622.
30. Hauser, M.A., Allingham, R.R., Linkroum, K., Wang, J., LaRocque-Abramson, K., Figueiredo, D., Santiago-Turla, C., del Bono, E.A., Haines, J.L., Pericak-Vance, M.A. *et al.* (2006) Distribution of WDR36 DNA sequence variants in patients with primary open-angle glaucoma. *Invest. Ophthalmol. Vis. Sci.*, **47**, 2542–2546.
31. Hewitt, A.W., Dimasi, D.P., Mackey, D.A. and Craig, J.E. (2006) A glaucoma case–control study of the WDR36 gene D658G sequence variant. *Am. J. Ophthalmol.*, **142**, 324–325.
32. Pasutto, F., Mardin, C.Y., Michels-Rautenstrauss, K., Weber, B.H., Sticht, H., Chavarria-Soley, G., Rautenstrauss, B., Kruse, F. and Reis, A. (2008) Profiling of WDR36 missense variants in German patients with glaucoma. *Invest. Ophthalmol. Vis. Sci.*, **49**, 270–274.
33. Fingert, J.H., Alward, W.L., Kwon, Y.H., Shankar, S.P., Andorf, J.L., Mackey, D.A., Sheffield, V.C. and Stone, E.M. (2007) No association between variations in the WDR36 gene and primary open-angle glaucoma. *Arch. Ophthalmol.*, **125**, 434–436.
34. Weisschuh, N., Wolf, C., Wissinger, B. and Gramer, E. (2007) Variations in the WDR36 gene in German patients with normal tension glaucoma. *Mol. Vis.*, **13**, 724–729.
35. Miyazawa, A., Fuse, N., Mengkegale, M., Ryu, M., Seimiya, M., Wada, Y. and Nishida, K. (2007) Association between primary open-angle glaucoma and WDR36 DNA sequence variants in Japanese. *Mol. Vis.*, **13**, 1912–1919.
36. Mao, M., Biery, M.C., Kobayashi, S.V., Ward, T., Schimmack, G., Burchard, J., Schelter, J.M., Dai, H., He, Y.D. and Linsley, P.S. (2004) T lymphocyte activation gene identification by coregulated expression on DNA microarrays. *Genomics*, **83**, 989–999.
37. Altschul, S.F., Gish, W., Miller, W., Myers, E.W. and Lipman, D.J. (1990) Basic local alignment search tool. *J. Mol. Biol.*, **215**, 403–410.
38. Bernstein, K.A., Gallagher, J.E., Mitchell, B.M., Granneman, S. and Baserga, S.J. (2004) The small-subunit processome is a ribosome assembly intermediate. *Eukaryot. Cell*, **3**, 1619–1626.
39. Dragon, F., Gallagher, J.E., Compagnone-Post, P.A., Mitchell, B.M., Porwancher, K.A., Wehner, K.A., Wormsley, S., Settlage, R.E., Shabanowitz, J., Osheim, Y. *et al.* (2002) A large nucleolar U3 ribonucleoprotein required for 18S ribosomal RNA biogenesis. *Nature*, **417**, 967–970.
40. Amsterdam, A., Nissen, R.M., Sun, Z., Swindell, E.C., Farrington, S. and Hopkins, N. (2004) Identification of 315 genes essential for early zebrafish development. *Proc. Natl Acad. Sci. USA*, **101**, 12792–12797.
41. Stevens, B., Allen, N.J., Vazquez, L.E., Howell, G.R., Christopherson, K.S., Nouri, N., Micheva, K.D., Mehalow, A.K., Huberman, A.D., Stafford, B. *et al.* (2007) The classical complement cascade mediates CNS synapse elimination. *Cell*, **131**, 1164–1178.
42. Stasi, K., Nagel, D., Yang, X., Wang, R.F., Ren, L., Podos, S.M., Mittag, T. and Danias, J. (2006) Complement component 1Q (C1Q) upregulation in retina of murine, primate, and human glaucomatous eyes. *Invest. Ophthalmol. Vis. Sci.*, **47**, 1024–1029.
43. Kuehn, M.H., Kim, C.Y., Ostojic, J., Bellin, M., Alward, W.L., Stone, E.M., Sakaguchi, D.S., Grozdanic, S.D. and Kwon, Y.H. (2006) Retinal

synthesis and deposition of complement components induced by ocular hypertension. *Exp. Eye Res.*, **83**, 620–628.
44. Udvadia, A.J., Koster, R.W. and Skene, J.H. (2001) GAP-43 promoter elements in transgenic zebrafish reveal a difference in signals for axon growth during CNS development and regeneration. *Development*, **128**, 1175–1182.
45. Venema, J. and Tollervey, D. (1999) Ribosome synthesis in *Saccharomyces cerevisiae*. *Annu. Rev. Genet.*, **33**, 261–311.
46. Azuma, M., Toyama, R., Laver, E. and Dawid, I.B. (2006) Perturbation of rRNA synthesis in the bap28 mutation leads to apoptosis mediated by p53 in the zebrafish central nervous system. *J. Biol. Chem.*, **281**, 13309–13316.
47. Boisvert, F.M., van Koningsbruggen, S., Navascues, J. and Lamond, A.I. (2007) The multifunctional nucleolus. *Nat. Rev. Mol. Cell Biol.*, **8**, 574–585.
48. Chen, J., Ruan, H., Ng, S.M., Gao, C., Soo, H.M., Wu, W., Zhang, Z., Wen, Z., Lane, D.P. and Peng, J. (2005) Loss of function of def selectively up-regulates Delta113p53 expression to arrest expansion growth of digestive organs in zebrafish. *Genes. Dev.*, **19**, 2900–2911.
49. Bourdon, J.C., Fernandes, K., Murray-Zmijewski, F., Liu, G., Diot, A., Xirodimas, D.P., Saville, M.K. and Lane, D.P. (2005) p53 isoforms can regulate p53 transcriptional activity. *Genes. Dev.*, **19**, 2122–2137.
50. Langheinrich, U., Hennen, E., Stott, G. and Vacun, G. (2002) Zebrafish as a model organism for the identification and characterization of drugs and genes affecting p53 signaling. *Curr. Biol.*, **12**, 2023–2028.
51. Andersen, J.S., Lyon, C.E., Fox, A.H., Leung, A.K., Lam, Y.W., Steen, H., Mann, M. and Lamond, A.I. (2002) Directed proteomic analysis of the human nucleolus. *Curr. Biol.*, **12**, 1–11.
52. Dundr, M., Misteli, T. and Olson, M.O. (2000) The dynamics of postmitotic reassembly of the nucleolus. *J. Cell Biol.*, **150**, 433–446.
53. Berghmans, S., Murphey, R.D., Wienholds, E., Neuberg, D., Kutok, J.L., Fletcher, C.D., Morris, J.P., Liu, T.X., Schulte-Merker, S., Kanki, J.P. *et al.* (2005) tp53 mutant zebrafish develop malignant peripheral nerve sheath tumors. *Proc. Natl Acad. Sci. USA*, **102**, 407–412.
54. Chakarova, C.F., Hims, M.M., Bolz, H., Abu-Safieh, L., Patel, R.J., Papaioannou, M.G., Inglehearn, C.F., Keen, T.J., Willis, C., Moore, A.T. *et al.* (2002) Mutations in HPRP3, a third member of pre-mRNA splicing factor genes, implicated in autosomal dominant retinitis pigmentosa. *Hum. Mol. Genet.*, **11**, 87–92.
55. Maita, H., Kitaura, H., Keen, T.J., Inglehearn, C.F., Ariga, H. and Iguchi-Ariga, S.M. (2004) PAP-1, the mutated gene underlying the RP9 form of dominant retinitis pigmentosa, is a splicing factor. *Exp. Cell Res.*, **300**, 283–296.
56. McKie, A.B., McHale, J.C., Keen, T.J., Tarttelin, E.E., Goliath, R., van Lith-Verhoeven, J.J., Greenberg, J., Ramesar, R.S., Hoyng, C.B., Cremers, F.P. *et al.* (2001) Mutations in the pre-mRNA splicing factor gene PRPC8 in autosomal dominant retinitis pigmentosa (RP13). *Hum. Mol. Genet.*, **10**, 1555–1562.
57. Vithana, E.N., Abu-Safieh, L., Allen, M.J., Carey, A., Papaioannou, M., Chakarova, C., Al-Maghtheh, M., Ebenezer, N.D., Willis, C., Moore, A.T. *et al.* (2001) A human homolog of yeast pre-mRNA splicing gene, PRP31, underlies autosomal dominant retinitis pigmentosa on chromosome 19q13.4 (RP11). *Mol. Cell*, **8**, 375–381.
58. Choesmel, V., Bacqueville, D., Rouquette, J., Noaillac-Depeyre, J., Fribourg, S., Cretien, A., Leblanc, T., Tchernia, G., Da Costa, L. and Gleizes, P.E. (2007) Impaired ribosome biogenesis in Diamond-Blackfan anemia. *Blood*, **109**, 1275–1283.
59. Wang, C., Query, C.C. and Meier, U.T. (2002) Immunopurified small nucleolar ribonucleoprotein particles pseudouridylate rRNA independently of their association with phosphorylated Nopp140. *Mol. Cell Biol.*, **22**, 8457–8466.
60. Heiss, N.S., Knight, S.W., Vulliamy, T.J., Klauck, S.M., Wiemann, S., Mason, P.J., Poustka, A. and Dokal, I. (1998) X-linked dyskeratosis congenita is caused by mutations in a highly conserved gene with putative nucleolar functions. *Nat. Genet.*, **19**, 32–38.
61. Kerrigan, L.A., Zack, D.J., Quigley, H.A., Smith, S.D. and Pease, M.E. (1997) TUNEL-positive ganglion cells in human primary open-angle glaucoma. *Arch. Ophthalmol.*, **115**, 1031–1035.
62. Nickells, R.W. (2007) Ganglion cell death in glaucoma: from mice to men. *Vet. Ophthalmol.*, **10** (Suppl 1), 88–94.
63. Acharya, M., Mitra, S., Mukhopadhyay, A., Khan, M., Roychoudhury, S. and Ray, K. (2002) Distribution of p53 codon 72 polymorphism in Indian primary open angle glaucoma patients. *Mol. Vis.*, **8**, 367–371.
64. Lin, H.J., Chen, W.C., Tsai, F.J. and Tsai, S.W. (2002) Distributions of p53 codon 72 polymorphism in primary open angle glaucoma. *Br. J. Ophthalmol.*, **86**, 767–770.
65. Dimasi, D.P., Hewitt, A.W., Green, C.M., Mackey, D.A. and Craig, J.E. (2005) Lack of association of p53 polymorphisms and haplotypes in high and normal tension open angle glaucoma. *J. Med. Genet.*, **42**, e55.
66. Ressiniotis, T., Griffiths, P.G., Birch, M., Keers, S. and Chinnery, P.F. (2004) Primary open angle glaucoma is associated with a specific p53 gene haplotype. *J. Med. Genet.*, **41**, 296–298.
67. Thisse, B., Heyer, V., Lux, A., Alunni, V., Degrave, A., Seiliez, I., Kirchner, J., Parkhill, J.P. and Thisse, C. (2004) Spatial and temporal expression of the zebrafish genome by large-scale *in situ* hybridization screening. *Methods Cell Biol.*, **77**, 505–519.
68. Thisse, C. and Thisse, B. (2008) High-resolution *in situ* hybridization to whole-mount zebrafish embryos. *Nat. Protoc.*, **3**, 59–69.
69. Winer, J., Jung, C.K., Shackel, I. and Williams, P.M. (1999) Development and validation of real-time quantitative reverse transcriptase–polymerase chain reaction for monitoring gene expression in cardiac myocytes *in vitro*. *Anal. Biochem.*, **270**, 41–49.
70. Kwan, K.M., Fujimoto, E., Grabher, C., Mangum, B.D., Hardy, M.E., Campbell, D.S., Parant, J.M., Yost, H.J., Kanki, J.P. and Chien, C.B. (2007) The Tol2kit: a multisite gateway-based construction kit for Tol2 transposon transgenesis constructs. *Dev. Dyn.*, **236**, 3088–3099.
71. Soules, K.A. and Link, B.A. (2005) Morphogenesis of the anterior segment in the zebrafish eye. *BMC Dev. Biol.*, **5**, 12.
72. Murphey, R.D., Stern, H.M., Straub, C.T. and Zon, L.I. (2006) A chemical genetic screen for cell cycle inhibitors in zebrafish embryos. *Chem. Biol. Drug Des.*, **68**, 213–219.